Published in final edited form as:
Dev Dyn. 2011 June ; 240(6): 1613–1625. doi:10.1002/dvdy.22644.

Tumor suppressor Lzap regulates cell cycle progression, doming and zebrafish epiboly

Dan Liu[1], **Wen-Der Wang**[2,§], **David B. Melville**[2], **Yong I. Cha**[3,4], **Zhirong Yin**[5], **Natalia Issaeva**[5], **Ela W. Knapik**[2,*], and **Wendell G. Yarbrough**[1,3,5,*]

[1]Department of Cancer Biology, Vanderbilt University, Nashville, Tennessee, USA

[2]Departments of Medicine, and Cell and Developmental Biology, Vanderbilt University, Nashville, Tennessee, USA

[3]Vanderbilt-Ingram Cancer Center, Vanderbilt University, Nashville, Tennessee, USA

[4]Department of Radiation Oncology, Vanderbilt University, Nashville, Tennessee, USA

[5]Department of Otolaryngology, Vanderbilt University, Nashville, Tennessee, USA

Abstract

Initial stages of embryonic development rely on rapid, synchronized cell divisions of the fertilized egg followed by a set of morphogenetic movements collectively called epiboly and gastrulation. Lzap is a putative tumor suppressor whose expression is lost in 30% of head and neck squamous cell carcinomas. Lzap activities include regulation of cell cycle progression and response to therapeutic agents. Here we explore developmental roles of the *lzap* gene during zebrafish morphogenesis. Lzap is highly conserved among vertebrates and is maternally deposited. Expression is initially ubiquitous during gastrulation, and later becomes more prominent in the pharyngeal arches, digestive tract and brain. Antisense morpholino-mediated depletion of Lzap resulted in delayed cell divisions and apoptosis during blastomere formation, resulting in fewer, larger cells. Cell cycle analysis suggested that Lzap loss in early embryonic cells resulted in a G2/M arrest. Furthermore, the Lzap-deficient embryos failed to initiate epiboly – the earliest morphogenetic movement in animal development – which has been shown to be dependent on cell adhesion and migration of epithelial sheets. Our results strongly implicate Lzap in regulation of cell cycle progression, adhesion and migratory activity of epithelial cell sheets during early development. These functions provide further insight into Lzap activity that may contribute not only to development, but also to tumor formation.

Keywords

Lzap; zebrafish; epiboly; cell cycle; tumor suppressor

INTRODUCTION

Lzap (also called CDK5Rap3 or C53) was first discovered as a binding partner of the 35kDa CDK5 activator binding protein p35 (Ching et al., 2000). Activity of Lzap in association with p35 has not been further characterized and may not represent a major Lzap

[*]Correspondence to: Wendell G. Yarbrough, M.D., Vanderbilt University Medical Center, Department of Otolaryngology, 2200 Pierce Ave, 654 Preston Research Building, Nashville, TN 37232-0275, USA. wendell.g.yarbrough@vanderbilt.edu.
[*]Contributed equally as senior authors
[§]Current address: Department of Bioagricultural Science, National Chiayi University, Chiayi, Taiwan

functionality since CDK5 and p35 expression is restricted to central nervous system neurons in mammals. Lzap is ubiquitously expressed in most organs, including: pancreas, brain, liver, heart, intestine, spleen, thymus, muscle and lung (Ching et al., 2000; Wang et al., 2006; and data not shown). Functionally, the Lzap protein binds to the Alternate Reading Frame protein of the INK4a gene locus ($p14^{ARF}$ in humans and $p19^{ARF}$ in mice) and enhances p53 activity in the presence or absence of ARF. Increased p53 activity following Lzap expression results in expression of the cyclin-dependent kinase inhibitor p21 and G1 cell cycle arrest (Wang et al., 2006). Lzap also binds and inhibits RelA resulting in decreased cellular invasion, decreased anchorage independent growth and decreased transcription of selective NF-κB targets including IL-8 (Wang et al., 2007). Furthermore, Lzap binds and inhibits the checkpoint kinases, Chk1 and Chk2, which leads to inappropriate or early progression through the G2 and M phase of the cell cycle and increased sensitivity to chemotherapeutic agents (Jiang et al., 2005; Jiang et al., 2009).

Remarkably, Lzap protein expression is markedly decreased in approximately 30% of head and neck squamous cell carcinomas (HNSCC). *In vivo*, loss of Lzap accelerates tumor xenograft growth, and tumors lacking Lzap have increased expression of RelA targets and increased vascularity (Wang et al., 2007). Lzap contains no identifiable enzymatic domains or other known motifs to suggest enzymatic activity, indicating that Lzap activity may be mediated through protein-protein interaction.

Loss of Lzap expression in HNSCC and cellular consequences of Lzap activities suggest that Lzap has tumor suppressor-like qualities; however developmental roles of Lzap remain unknown. Loss of Lzap renders cells, at least partially, resistant to genotoxin-induced apoptosis possibly through increasing ability to arrest and repair before mitotic entry. Lzap knockdown delays CDK1 activation and mitotic entry possibly related to increased Chk1 and Chk2 activity, and results in dysreguation of cell cycle progression in tumor cell lines (Jiang et al., 2005; Jiang et al., 2009).

Mechanisms to explain biological activities of Lzap continue to emerge. We have recently found that Lzap binds and inhibits activity of mitogen-activated protein kinase p38MAPK, suggesting another mechanism through which Lzap could alter proliferation and cell death (An et al., 2011). To further investigate the functions of Lzap *in vivo*, we generated transgenic mice with targeted Lzap. In these studies, heterozygous ($Lzap^{+/-}$) mice were born, developed normally, and are currently being analyzed for inflammatory and tumorigenic phenotypes. Of note, live birth of homozygous knockout mice ($Lzap^{-/-}$) has not been observed, suggesting that homozygous loss of Lzap results in embryonic lethality in mice (data not shown).

The absence of live births of $Lzap^{-/-}$ mice led us to explore developmental defects resulting from Lzap loss. Zebrafish is a vertebrate whose eggs are externally fertilized, thus providing an opportunity to examine the earliest cell behaviors in the live embryos. This feature, combined with zebrafish's rapid development and transparent embryos, allowed detailed *in vivo* description of epiboly and gastrulation movements (Kane and Kimmel, 1993; Montero et al., 2003; Solnica-Krezel, 2006).

During the first 3 hours of zebrafish development, cells are replicating DNA and rapidly dividing, resulting in an increasing number of progressively smaller cells. Approximately 3 hours post-fertilization (hpf), zygotic transcription begins, in a process referred to as the midblastula transition (MBT). Cells are not motile before MBT (Kane and Kimmel, 1993), but within an hour they form three distinct layers: two extraembryonic lineages – an outer enveloping layer (EVL) and an inner dual layer, consisting of the yolk syncytial layer (YSL) and yolk cytoplasmic layer (YCL) – and the embryo proper between the EVL and the YSL/

YCL. These embryonic cells, which are referred to as the deep cell layer (DCL), will give rise to ectoderm, endoderm and mesoderm through the morphogenetic movements of gastrulation. Epiboly is the first morphogenetic movement. It converts a ball of dividing cells into a sheet of cells spreading over the yolk (Arendt and Nubler-Jung, 1999; Solnica-Krezel, 2005). The first visible sign of epiboly appears around 4 hpf with the flattening of the blastoderm and doming of the yolk. As epiboly progresses, cells of EVL and forming epiblast behave as tightly packed epithelia with extended cell-cell interactions and continuous spatial rearrangements (Solnica-Krezel, 2005; Lachnit et al., 2008). Normal physiological cell death has not been observed during these stages; however, when the process of epiboly is stalled, developing embryos will die unable to initiate gastrulation. Although a number of genes were implicated in enabling epiboly, e.g. E-cadherin (Kane et al., 2005), G proteins (Lin et al., 2009), prostaglandin E_2 (Cha et al., 2006), and Pou5f1 (Lachnit et al., 2008), molecular mechanisms controlling epiboly are only beginning to be explored.

To begin defining the physiological role of Lzap in embryogenesis, morpholino (MO)-directed loss of Lzap in zebrafish was performed and development was observed. The spatio-temporal expression of *lzap* was determined, revealing maternal deposition and high levels of expression during the initial cleavage stages. In organogenesis, *lzap* was highly expressed in pharyngeal arches, digestive tract, and brain. MO-mediated loss of Lzap function (*lzap* MO) resulted in slowed progression of cell division during blastomere cleavage stages and absence of epiboly in the majority of morphant embryos. Analysis of PCNA, phospho-histone H3 and activated Caspase-3 indicated decreased proliferation and mitosis but increased apoptosis in Lzap-depleted embryos. Cell cycle analysis of embryonic cells suggested that loss of Lzap resulted in a G2/M arrest. H&E histological staining revealed loosely packed blastoderm cells indicative of disrupted cell-cell adhesion. These results strongly suggest that Lzap is essential for cell cycle progression and that loss of Lzap results in poorly adherent cells and inhibition of epiboly.

RESULTS AND DISCUSSION

Lzap is Highly Conserved Across Species

Using *in silico* data mining of NCBI databases, sequences encoding Lzap orthologues were aligned, revealing that they are highly conserved in vertebrates, invertebrates and plants but not in unicellular yeast and bacteria. The zebrafish *lzap* gene spans 9.3 Kb of genomic sequence and is located on zebrafish chromosome 12 (Fig. 1A). The full-length cDNA of the *lzap* gene was amplified using gene-specific primers and total RNA from zebrafish wild-type AB strain as template. A 1524 bp transcript comprised the full-length cDNA and encoded a protein consisting of a predicted 507 amino acid residues. Sequence alignment demonstrated that the zebrafish Lzap protein is highly similar in composition and length to the human and murine orthologues. Similarity between zebrafish Lzap and either human or murine Lzap is greater than 80%, and between murine and human Lzap is more than 90%, indicating that structural, and likely functional aspects of Lzap have been highly conserved during evolution (Fig. 1B, and Fig. 1C). Sequence alignment suggests that the amino-terminal portion (amino acids 1–122) and carboxyl-terminal (amino acids 412-terminus of Lzap) domain are even more faithfully conserved, suggesting that these stretches of amino acids may represent important functional domains of the protein.

lzap is Expressed during Epiboly and Organogenesis

To determine timing and relative magnitude of *lzap* expression during development, qRT-PCR using exon-spanning *lzap*-specific primers was performed on total RNA isolated from whole embryos at developmental stages ranging between 1-cell stage and 5 days post

fertilization (dpf) (Fig. 2A). *lzap* was expressed during all developmental stages examined. When normalized to *β-actin*, *lzap* expression decreased during gastrulation. Interestingly, our results indicate that expression of *lzap* is dramatically up-regulated at 12 hours post-fertilization (hpf). Since there is no ideal gene for normalization during very early development (Tang et al., 2007), and *β-actin* expression is low at 1-cell stage and increases with development in a time-dependent manner before shield stage (Cao et al., 2004; Duffy et al., 2005), the normalized quantification of expressed *lzap* during very early development (<6 hpf) may be overestimated. To begin exploring cellular, tissue, and organ localization of *lzap* transcripts, we performed *in situ* hybridization on zebrafish whole mount embryos representing the same developmental stages as examined by qRT-PCR (Fig. 2B–L). Maternal deposition and ubiquitous expression of *lzap* was observed throughout cleavage stages (Fig. 2B–C). *lzap* was widely expressed in early epiboly (Fig. 2D), but at 12 hpf expression of *lzap* was restricted to the prechordal plate in an area corresponding to hatching gland at Prim stages (Fig. 2E–G). *lzap* expression was first detected in the CNS, eye and mesoderm at 24 hpf, and expression persisted throughout the second day of development (Fig. 2G and 2H). At 3 dpf, *lzap* transcripts were detectable in the region of the developing pharynx, pharyngeal arches and in the primordia of the gastrointestinal organs (Fig. 2I). As development progressed, *lzap* expression persisted in the pancreas and gastrointestinal tube, jaw and pharynx region, tectum, and the hindbrain regions (Fig. 2J and 2K). Specifically, *lzap* expression appears to be present in pharyngeal arch epithelia at 4 and 5 dpf, in structures that will contribute to future gills (Fig. 2K). The 1.6 Kb-long anti-sense RNA probe used for *in situ* hybridization experiments spanned the full-length cDNA. The equivalent probe transcribed in the sense orientation was used as a control and did not detect expression (Fig. 2L).

Morpholino-mediated Depletion of Lzap Results in Epiboly Defects

To investigate the function of Lzap during development, we generated loss-of-function zebrafish morphants by injection of antisense oligonucleotides into 1-cell stage embryos to block protein translation. The *lzap* morpholino (MO) corresponded to sequences within the 5’ untranslated region (UTR) and was designed to target both maternal and zygotic transcripts. A MO corresponding to the *lzap* 5’ UTR targeting MO but with a 5 bp mismatch was used as control. Several antibodies recognizing mammalian Lzap were tested for reactivity with zebrafish Lzap protein; however, they did not recognize zebrafish Lzap by either immunoblotting or immunostaining. In addition, full-length zebrafish Lzap was used to make rabbit polyclonal antibodies. Unfortunately, initial bleeds of the rabbits revealed no specific antibodies. Therefore, to determine effectiveness and specificity of the 5’ UTR MO, an expression construct that included the 5’ UTR sequence targeted by the MO, the *lzap* open reading frame, and three HA tags at the C-terminus (*lzap:3HA*, Fig. 3A) was used to measure effectiveness of Lzap MO. Expression of HA-tagged Lzap from the *lzap:3HA* construct was detectable in 89% of injected embryos by 4 hpf without developmental dysmorphology, as assessed by direct immunofluorescence with antibodies against the HA tag. To estimate the minimal effective concentration of MO capable of inhibiting Lzap expression, *in vitro* synthesized *lzap:3HA* mRNA and increasing MO doses (2 ng, 4 ng, or 6 ng) were co-injected, and HA-tagged Lzap expression determined by immunofluorescence (Fig. 3B). Following injection of 2 ng MO, expression of HA-tagged Lzap was decreased in approximately 50% of injected embryos and was undetectable in the remainder. Following injection of 4 ng and higher concentrations of *lzap* MO, HA-tagged Lzap could not be detected by immunofluorescence in essentially any injected embryos. Since 4 ng of *lzap* MO was the lowest effective dose that consistently ablated exogenous Lzap expression, it was used in all following experiments.

Consistent with early expression of Lzap (Fig. 2), the morphant phenotype was observed before the midblastula transition (MBT), the time marking onset of zygotic transcription. At 3 hpf, *lzap* morphants could be categorized as: (i) normally developing embryos (18%), (ii) dead embryos (33%), and (iii) abnormal embryos (49%). Abnormal morphant embryos could be further categorized as either mildly or severely abnormal (Fig. 3C). At 3 hpf, development of morphant embryos with a mild phenotype lagged the wild-type embryos by approximately 40 minutes, and the severely abnormal morphants were even further delayed (Fig. 3D—3D"). At 6 hpf, nearly all MO injected embryos presented a phenotype, and 56% of injected embryos were dead. Surviving morphant embryos at 6 hours failed to dome, which normally occurs at 4 hpf, and remained at the sphere stage (Fig. 3E-E"). In animals with mild phenotype, epiboly proceeded up to the yolk plug closure, albeit at a slower pace than in uninjected controls. Of *lzap* morphant embryos, the severe phenotype was most common with embryos reaching oblong stage (3.7 hpf, Fig. 3E"), where they persisted for up to 12 hpf before degenerating. In contrast, the mild category morphants completed gastrulation, undergoing involution, dorsal convergence and limited extension before dying between 12 and 24 hpf. The majority (80%) of the embryos injected with comparable dose of the control MO developed normally (Fig. 3C), and no differences were observed between uninjected embryos and embryos injected with control MO.

Epiboly Defects in *lzap* Morphants can be Rescued by Co-injection of *lzap* mRNA

To exclude off target effects and to verify MO specificity, as well as to implicate Lzap in the extensive developmental delay observed in *lzap* morphants, rescue experiments were performed using synthetic *lzap:CDs* mRNA that contained full-length *lzap* open reading frame but lacked MO target sequences within the 5' UTR (Fig. 3A). Injection of 100 pg of the capped *lzap:CDs* mRNA did not result in developmental dysmorphology (not shown), but co-injection with 4 ng of *lzap* MO significantly improved morphants' survival during the first 24 hours of development and accelerated gastrulation to almost normal rates (Fig. 4A–4F, S1 and data not shown). Morphant rescue with *lzap* mRNA increased the percentage of live embryos from 67% to 94% at 3 hpf, from 44% to 81% at 6 hpf and from 12% to 38% at 24 hpf (Fig. 4G). There was a significant loss of embryo viability in the rescued group co-injected with *lzap* MO and *lzap* mRNA between 6 hpf and 24 hpf; however, compared to the *lzap* MO group, embryo viability following *lzap* mRNA remained significantly improved. It is possible that expression of Lzap may inhibit cellular or embryo viability between 6 and 24 hpf. Alternatively, lethality following co-injection of *lzap* MO and mRNA may be due to longer stability of MO compared to co-injected synthetic mRNA. Taken together, these results indicate that the observed phenotypes are due to depletion of Lzap and suggest that endogenous Lzap expression is critical for normal development and survival in the early embryo.

We and others have previously shown that Lzap regulates mitotic entry, cell cycle progression and genotoxin-induced apoptosis, likely through its interaction or regulation proteins involved in apoptosis and cell cycle: p53, p38, Chk1/2 and CDK1 (Jiang et al., 2005; Wang et al., 2006; and data not shown). To begin exploring potential cellular mechanisms mediating Lzap function, we analyzed cellular proliferation, mitosis and apoptosis in *lzap* MO-injected and rescued embryos. At 6 hpf, proliferation of embryonic cells was approximated by expression of PCNA, mitosis by expression of phospho-histone H3 (p-Histone H3), and apoptosis by expression of activated (cleaved) Caspase-3. Three groups of uninjected-, 4 ng MO injected-, and 4 ng MO / 100 pg *lzap* RNA co-injected-embryos were collected for analysis at 6 hpf (Fig. 4H).

PCNA is a subunit of DNA polymerase that plays a critical role in DNA replication. Cells were scored as proliferating only if PCNA staining was detected within the nucleus. Proliferative index was calculated by dividing PCNA positive cells by total number of cells

examined within the 3 groups of embryos (Fig. 4I). At 6 hpf, cells with PCNA expression were observed throughout embryos in uninjected controls, *lzap* morphants, and *lzap* mRNA rescue groups; however, the proliferative index of *lzap* morphants was significantly decreased compared to controls (92% vs. 56%, $p<0.01$). Proliferative index was partially restored (56% vs. 77%, $p<0.01$) following rescue through co-injection of *lzap* mRNA with MO (Fig. 4H and 4I).

To further support findings of differences in cellular proliferation as indicated by PCNA expression, expression of p-Histone H3 as a marker of mitosis was determined using immunohistochemistry (IHC). Mitotic index was defined by dividing the number of p-Histone H3-positive cells by the total number of cells examined (Fig. 4H and 4J). Consistent with proliferation data as measured by PCNA, the mitotic index revealed that mitoses were significantly reduced in *lzap* morphants compared to controls (16% vs. 6%, $p<0.01$). Rescue by co-injection of *lzap* mRNA significantly increased mitosis compared to *lzap* morphants (6% vs. 11%, $p<0.05$) but did not restore mitotic index to the level observed in control embryos (11% vs. 16%, $p<0.05$).

To measure apoptosis within embryos, IHC was performed using antibodies specific to cleaved Caspase-3, and apoptotic index was determined by dividing Caspase-3 positive cell number by total number of cells examined (Fig. 4H and K). Consistent with reports which show that during normal development apoptosis is not observed prior to gastrulation (Yamashita, 2003; Granero-Molto et al., 2008), we observed no apoptosis in control embryos at 6 or 24 hpf (Fig. 4H and S2). However, following *lzap* MO injection, 7% of cells expressed cleaved Caspase-3 as a marker of apoptosis (0% vs. 7%, $p < 0.01$). Co-injection of *lzap* morphants with *lzap* mRNA significantly decreased the apoptotic index from 7% to 2% ($p < 0.05$). The presence of apoptosis in *lzap* morphants at 6 and 12 hpf was confirmed by TUNEL assay (Fig. S2). These data suggest that MO-directed knockdown of Lzap during early embryogenesis increased activity of the intrinsic apoptosis pathway resulting in early and increased apoptosis. Although potentially contributing to embryonic lethality, it should be recognized that the relatively low levels of cellular apoptosis observed in *lzap* morphant embryos may not be the sole contributor to embryonic death in *lzap* morphants. Although not explored, it is possible that necrosis may contribute to observed early embryonic death given reports describing necrosis in embryos failing to initiate epiboly, regardless of the precipitating defect responsible for inhibition of epiboly (Kishimoto et al., 2004; Reim and Brand, 2006).

In addition to cellular phenotypes of proliferation, mitosis and apoptosis, histological evaluation of morphant embryos revealed a noticeable difference in cell number, cell size and cell adhesion compared to control embryos (Fig. 4H). Relative cell size was quantified by ImageJ software (NIH) using microscopic images of control, morphant and rescued embryos based on H&E stained sections at 6 hpf (Fig. 4H). The mean cell size for morphant embryos was significantly greater when compared to cells from control embryos (1.5 fold, $p<0.05$) (Fig. 4L). Although rescue with *lzap* mRNA partially corrected proliferation, mitosis and apoptosis defects caused by *lzap* MO, expression of *lzap* did not restore the cell size abnormality observed in the morphant embryos. Larger cell size and fewer nuclei were observed throughout the first 6 hpf, suggesting that Lzap may be required for normal cell cycle progression.

Dividing cells before the MBT are not motile, but within an hour after onset of MBT, they begin epiboly that generates a sheet of epithelial-like cells. This cellular layer provides material for morphogenetic movements of gastrulation with resultant formation of germ layers. Motility of these cells has been shown to be dependent on cell adhesion molecules including E-cadherin (Kane et al., 2005; Shimizu et al., 2005). Notably, sections of early

lzap morphant embryos revealed gaps between cells, which were not seen in controls or in morphants rescued by injection of *lzap* mRNA. Although intercellular spaces observed in *lzap* morphant embryos could be an artifact of fixation, the fact that it was not observed in control or rescued embryos suggests that loss of *lzap* may alter intercellular adhesion, potentially contributing to abrogation of epiboly. These observations suggest that Lzap may play a role in both proliferation and in cell adhesion and progress of epiboly.

Lzap is Required for Normal Cell Cycle, but not Zygotic Gene Expression after MBT

The MBT is marked by onset of zygotic gene expression with loss of synchronous cell division. To determine whether onset of zygotic transcription is disrupted by Lzap depletion, we have examined several genes that initiate expression after MBT at 6 hpf. Expression of zygotic genes *bmp2b*, *eve1*, and *ntl/brachyury* was initiated in age-matched zebrafish embryos in blastomeres at 6 hpf, and in older, stage-matched mild morphants, the expression was indistinguishable from control embryos (Joly et al., 1993; Schulte-Merker et al., 1994; Martinez-Barbera et al., 1997; Sidi et al., 2003; Ramel et al., 2005; Wilm and Solnica-Krezel, 2005) (Fig. 5A). The expression of anterior mesendoderm and hatching gland marker *hgg1/cathepsin L 1b*, in the polster is present in stage-matched mild morphants (McFarland et al., 2005) (Fig. 5A). However, the expression domain is smaller as compared to controls. Thus, zygotic transcription is initiated in Lzap depleted embryos.

To investigate changes in cell cycle progression associated with Lzap loss, *lzap* morphant embryos were dissociated and cell cycle position of embryonic cells was as determined by flow cytometry after propidium iodide labeling at 4 hpf. As expected based on PCNA staining of early embryos (Fig. 4H), control and *lzap* morphant embryos were rapidly proliferating and primarily in S phase (51% vs. 53%). However, *lzap* morphants had an increased G2/M population and a decreased G1 population relative to control (Fig. 5B-a). To better define the possible G2 delay, nocodazole was used to arrest cells in mitosis prior to release. In embryos treated with nocodazole for 30 min without release, G1 was similar between *lzap* morphants and controls, suggesting that loss of *lzap* does not have a major impact on progression through G1. As observed in untreated cells, *lzap* morphants treated with nocodazole had increased percentage of cells in G2/M (Fig. 5B-b). After release from nocodazole block for 15 min, control cells progressed primarily to G1, whereas *lzap* morphant cells remained in G2/M (Fig. 5B-c). Following a 30 min release control cells had progressed out of G1 into S and were repopulating G2/M. In contrast, following 30 min release, *lzap* morphant were primarily in G1 and S, but had not begun to repopulate G2 (Fig. 5B-d). Although minor defects in G1 progression of cells derived from *lzap* morphants cannot be excluded, these data are consistent with a G2/M arrest associated with *lzap* loss. Analyses also revealed an increased sub-G1 population in *lzap* morphants consistent with increased apoptosis as observed by Caspase-3 staining (Fig. 4H and data not shown).

In parallel, we investigated cell division by immunofluorescence at three consecutive stages (4h, 6h, 9h) past MBT. We labeled mitotic spindles using α-tubulin antibody and condensed chromatin at metaphase and early anaphase by p–Histone H3 antibody (Fig. 5C). We have analyzed overall size and shape of nuclei by TO-PRO-3 labeling and confocal imaging of whole mount preparations. We found that the nuclei are of comparable size and number at 4 hpf in morphants and controls, however at 6 and 9 hpf the size and number of *lzap* morphant nuclei remain similar to the earlier stage while control nuclei increase in number and decrease in size (Fig. S3). The formation of mitotic spindles was not disturbed by Lzap depletion, and the chromosome alignment at metaphase was comparable between morphants and controls at all stages tested. Despite the distinction of nuclear size and number following Lzap loss, there were no gross abnormalities of chromatin morphology such as nuclear strings connecting nuclei or fragmented chromatin. These results suggest that Lzap depletion does not interfere with assembly of mitotic spindles and chromatin condensation for mitosis.

CONCLUSIONS

The *lzap* gene structure and protein sequence are highly conserved across species which may be a result of its critical developmental role. Here, we present a set of experiments that query the role of Lzap during zebrafish development.

We show that Lzap is ubiquitously expressed during blastomere cleavage stages and gastrulation. Interestingly, homozygous Lzap knockout mice are embryonic lethal, and $Lzap^{-/-}$embryos could not be found from dissection of pregnant females at or after embryonic day 6.5 (unpublished data). These results are consistent with the phenotype of the zebrafish Lzap knockdown embryos that are lethal at an early embryonic stage, failing to initiate epiboly. Thus, both zebrafish and murine data suggest that Lzap is essential for early embryogenesis.

We and others have shown that Lzap can bind to or regulate proteins regulating cell cycle progression (e.g. p53, ARF p38, Chk1/2 and CDK1) (Jiang et al., 2005; Wang et al., 2006; Jiang et al., 2009). Through these effectors, Lzap has been shown to regulate mitotic entry, G2/M checkpoint, cell cycle progression and apoptosis. In zebrafish development, we show that loss of *lzap* increases apoptosis and inhibits proliferation.

Epiboly

Epiboly is the first morphogenetic movement that in zebrafish initiates approximately 1 h after the midblastula transition (MBT) with intercalation of the deep blastomeres and animalward movement of the yolk (doming). Actin inhibitors and calcium chelators interrupt epiboly, but few genes have been implicated in this process (Cheng et al., 2004). In *lzap* morphants, despite progression through the MBT with expression of zygotic genes and mesodermal markers, neither doming nor epiboly was observed. Previously, four mutants were identified that arrest epiboly at the stage greater than 60% (Kane et al., 1996). Depletion of Lzap arrests epiboly before any morphogenetic movements begin suggesting that Lzap is not likely to be altered in these epiboly mutants.

Zebrafish mutants that disrupt development prior to the MBT have been isolated by mutagenesis to screen for maternal effect genes; however, most of the genes have yet to be cloned and none of the described mutants mimic the *lzap* morphant phenotype (Dosch et al., 2004; Abrams and Mullins, 2009). Pre-MBT mutants including *irreducible* (*irr*), *indivisible* (*ini*), *atomos* (*aoo*), *cellular island* (*cei*) and *cellular atoll* (*cea*) each failed to initiate cytokinesis, karyokinesis or both, whereas *lzap* morphants do not display abnormalities in cytokinesis or karyokinesis. The large cell morphology observed in *lzap* morphants is reminiscent of the *screeching halt* (*srh*) mutant (Wagner et al., 2004). Similar to *srh* mutants, *lzap* morphants zygotically express *ntl*, *eve1* and *bmp2b*, in a spatial pattern consistent with failure to progress past the sphere stage in age-matched embryos, however in stage-matched morphants these genes are expressed in a normal pattern. Unlike *srh*, the *lzap* morphants present normal nuclear morphology, alignment of metaphase chromosomes and mitotic spindle formation (Fig. 5C and S3).

The zebrafish *betty boop* mutant (*bbp*) causes arrest of epiboly with constriction and bursting of the yolk cell at 50% epiboly. This defect was linked to an inactivating mutation of MAPKAPK2 (Holloway et al., 2009). MAPKAPK2 is a downstream target of the mitogen activated protein kinase p38 and dominant negative mutations of p38MAPK recapitulate the *bbp* phenotype. Likewise, mutations in the homeobox transcription factor, Mxtx2, resulted in a similar phenotype (Bruce et al., 2005; Wilkins et al., 2008). Although yolk bursting was not observed in *lzap* morphants, we have recently found that human Lzap

binds and inhibits p38MAPK suggesting that this pathway could be involved in epiboly defects observed in Lzap depleted animals (An et al., 2011).

Cell Cycle

In mammalian cells loss of Lzap results in cell cycle defects. To determine whether cell cycle progression was altered in *lzap* morphants, proliferative and mitotic indices and cell cycle position were determined in cells dissociated from early embryo (Fig. 4). Percentages of proliferating and mitotic cells were decreased in *lzap* morphant embryos. Flow cytometry of untreated embryos revealed that fewer cells from *lzap* morphants were in G1 and more cells were in G2/M, but analyses of unperturbed cells was limited because of the rapid cell cycle at this stage with the majority of cells positioned in S phase (Zamir et al., 1997). Nocodazole treatment and release was used to more finely determine cell cycle effects of Lzap loss (Fig. 5B). Following removal of nocodazole, *lzap* morphants were delayed in exit from the G2/M phase. Experiments performed do not rule out the possibility that cells are also delayed in G1 and S relative to control; however all results can be more simply explained by a G2/M delay. Polo-like kinase 1 (Plk1) and SCL-interrupting locus (SIL) are required for progression through mitosis and result in embryonic growth defects (Pfaff et al., 2007; Jeong et al., 2010). Both Plk1 and SIL result in disorganized mitotic spindles as opposed to *lzap* morphants whose spindles are morphologically normal (Fig. 5C).

Lzap loss in mammalian cells delays mitotic entry through activation of Chk1 and Chk2 consistent with our findings in unsynchronized cells. However, nocodazole results in a mitotic or spindle checkpoint arrest triggered by the presence of unattached kinetochores (Amon, 1999; Musacchio and Hardwick, 2002). Results presented here suggest that in addition to delaying exit from the G2 checkpoint, Lzap may also regulate exit from the spindle checkpoint.

Apoptosis

Interestingly, non-mammalian vertebrate embryos do not manifest spontaneous apoptosis before gastrulation; however, apoptotic machinery is present and apoptosis can be induced in zebrafish embryos post MBT by inhibition of protein or DNA replication (Ikegami et al., 1999; Negron and Lockshin, 2004). Mutation of *grp* and *Mei* in flies results in embryonic death, but apoptosis in these embryos has not been evaluated (Sibon et al., 1997; Sibon et al., 1999). Likewise, apoptosis was not examined in *screeching halt* zebrafish mutants (Wagner et al., 2004). Here, we show that *lzap* morphant embryos had a significant proportion of cellular apoptosis as early as 6 hpf (Fig. 4H, 4K and S2). Despite the ability of Lzap to activate p53 and p53's accepted role as an inducer of cell cycle arrest and apoptosis, concomitant loss of p53 did not affect severity of the *lzap* MO phenotype nor rescue *lzap* morphants (Fig. S4). Gaps between cells were commonly observed in 6 hpf *lzap* morphant embryos, less frequently observed in rescued morphants and not observed in control embryos. The mechanism responsible for loss of cell-cell adhesion has not been explored, but could relate to loss of adhesion molecules or may simply be a marker of impending cell death.

Combined, our data suggest that Lzap function is critical for progression to the G1 phase of the cell cycle and to prevent apoptosis in early embryos. Lzap also appears to be required for initiation of epiboly. Inhibition of doming and epiboly in *lzap* morphants is exciting and suggest that *lzap* activity is required at or before the earliest stages of cellular and tissue differentiation. The absence of initiation of doming or epiboly in *lzap* morphants is even more remarkable given that E-cadherin mutants with disrupted cell-cell adhesion still are capable of doming (Kane et al., 2005; Shimizu et al., 2005). Lzap deficient zebrafish embryos showed disrupted development at an earlier time point than fish with mutated E-

cadherin, MAPKAPK2, or p38MAPK or than in described epiboly mutants and at a stage where embryonic cells should maintain a pluripotency (Ma et al., 2001). These studies suggest that Lzap may be required for embryonic stem cell maintenance or appropriate cell fate determination.

EXPERIMENTAL PROCEDURES

Zebrafish Lines

Zebrafish, AB strain, were raised in the Vanderbilt Zebrafish Core Facility and maintained under standard conditions at 28°C according to the policies and procedures of the Institutional Animal Care and Use Committee of Vanderbilt University. Embryos were obtained by natural spawning and were staged according to (Kimmel et al., 1995).

Cloning of Zebrafish *lzap* cDNA and Sequence Analysis

A zebrafish Lzap ortholog (NP_001002105) was identified by NCBI Blink search using the sequence of the mouse Lzap ortholog (NP_084524.1). Total RNA was isolated from 1-cell to 120 hours post fertilization (hpf) wild-type embryos in TRI-Reagent (Sigma). cDNA was synthesized from 48 hpf RNA template by reverse transcription using the iScript cDNA synthesis Kit (Bio-Rad) according to the manufacturer's protocol. Transcripts of *lzap* were amplified by PfuTURBO DNA polymerase (Stratagene) and products were subcloned into pCR-Blunt II-TOPO (Invitrogen). Primers were as follows: *lzap*-coding region forward: 5'-ATGGAGAACATCCAGAATCT-3'; and reverse: 5'-TCACACATGAACTCCCATGA-3'. A second fragment containing the 5'-UTR and 3'-UTR regions were cloned using primers *lzap*-UTR forward: 5'-GTGGAAATGTAAACTTGTGC-3'; and reverse: 5'-TGATGCATATGTGCAGCTTG-3'. The identity of the cloned zebrafish *lzap* gene was verified by sequencing in the forward and reverse directions by the Vanderbilt Sequencing Facility.

Quantitative RT-PCR

Total RNA was extracted from approximately 100 embryos at different embryonic time points using the TRIzol reagent (Sigma). A total of 50 ng of RNA was used per 20 μL reaction and performed by iScript One-Step RT-PCR Kit with SYBR Green on a Bio-Rad iCycler IQ according to the manufacture instructions. Sequences of primers were as follows: *lzap*-3'-UTR forward: 5'-GTGAAGAAGGCGACTTGGTG-3'; and reverse: 5'-TGATGCATATGTGCAGCTTG-3'. β-*actin* was used as a baseline expression using primers forward: 5'-GACTCAGGATGCGGAAACTG-3'; and reverse: 5'-GAAGTCCTGCAAGATCTTCAC-3'. Three independent experiments in triplicates were performed using β-*actin* as internal control. ΔΔC(T) Method was used to analyze relative gene expression data. *lzap* expression fold change was normalized to β-*actin* and relative quantity was normalized to 1-cell stage.

Morpholino Oligonucleotides and mRNA Microinjections

Antisense morpholinos (MO) specifically targeting 5'-UTR and used to knockdown Lzap expression were designed and purchased from Gene Tools, LLC (Philomath, OR). The sequences of the oligonucleotides were as follows: *lzap*-5'-UTR MO: 5'-AAGAATTACTAAAACGACCCCATGC-3' (targets bases −54 to −30); and the corresponding 5-base pairs mismatch control morpholino: 5'-AACAATTAGTATAACCACCCCATCC-3'. Additional MO oligonucleotides were designed and purchased to target ATG start codon. The sequences of ATG MO are as follows: 5'-AGGGAGATTCTGGATGTTCTCCATT-3' (targets bases −1 to 24). This ATG MO at 8 ng caused the same morphologic phenotype as 5'UTR MO at 4 ng dose (Fig. S5),

therefore, we used the later in all presented experiments. The MOs were dissolved in distilled water and pressure-injected into the egg yolk of 1- to 2-cell stage embryos as described (Montero-Balaguer et al., 2006). The full-length cDNA of *lzap* was amplified by PCR and subcloned into the pCS2+ expression vector. Additional constructs used in this study: pCS2+-lzap:3HA (3× hemagglutinin tag added to the 3'-end of *lzap* coding sequence); pCS2+-lzap:CDs (*lzap* cDNA lacking the 5'UTR subcloned into pCS2+ vector) for rescue experiments. Capped RNA (cRNA) was synthesized from expression constructs using the mMessage mMachine kit (Ambion) according to the manufacturer's instructions and RNA quality was assayed using gel electrophoresis. RNA, MO, or both combined were injected into the yolk of 1-to 2-cell stage embryos. Effective and specific doses of MOs and cRNA were determined by titration, reporter constructs and rescue experiments. Used concentrations are provided with each experiment. A validated MO targeting zebrafish *p53* (5'-GCGCCATTGCTTTGCAAGAATTG-3') was obtained from Gene Tools (Robu et al., 2007).

Whole-Mount In Situ Hybridization

Whole-mount *in situ* hybridization using Dig-labeled RNA probes was performed as previously described (Barrallo-Gimeno et al., 2004). For probe synthesis, *lzap* was cloned into pCR-Blunt II-TOPO, the vector was linearized with BamH I and antisense probes were synthesized with T7 RNA polymerase (Ambion). Hybridization and washing were performed at 63°C.

Histological and Immunohistochemical Analysis

Staged zebrafish embryos were fixed overnight in 4% PFA then embedded in paraffin, sectioned at 5 μm thickness and stained with hematoxyline and eosin (H&E) for histological analysis. To determine cell proliferation, mitotic and apoptotic rates, immunohistochemical stain for proliferating cell nuclear antigen (1:15000 dilution, Sigma-Aldrich), p-Histone H3 (1:400 dilution, Cell Signaling Technology) and active Caspase-3 (1:300 dilution, BD Pharmingen™) were performed respectively as described previously (Yin et al., 2008). The immunostained slides were examined by light microscopy. The cell proliferation, mitosis and apoptosis were assessed as PCNA, p-Histone H3 and active Caspase-3 labeling index (LI) respectively. For each embryo, the index was defined as the percentage of immune-positive embryonic cells of PCNA, p-Histone H3 or active Caspase-3 in total embryonic cells respectively. For each LI, 20 representative embryos were evaluated at higher power magnification (40X), and the average was calculated. The data for the PCNA, p-Histone H3 or active Caspase-3 LI were presented as mean ± standard deviation (SD).

Immunofluorescent Staining and TUNEL Labeling

Whole mount immunofluorescent staining was performed as described (Pfaff et al., 2007) using polyclonal Ser-10 p-Histone H3 (1:750 dilution, Santa Cruz) and monoclonal α-tubulin (1:500 dilution, Sigma) detected with Alexa Fluor fluorescently conjugated secondary antibody (1:600 dilution, Molecular Probes). For nuclear counterstain, embryos were incubated with TO-PRO-3 (1:1000 dilution, molecular probes) for 30 min. Confocal images were taken with a Zeiss LSM510 inverted confocal microscopy (Vanderbilt Cell Imaging Shared Resource). For TUNEL staining, embryos were dechorionated and fixed at 6 and 12 hpf and apoptotic cells visualized by in-situ cell death detection kit (Roche).

FACS Analysis of DNA Content and Nocodazole Treatment

MO-injected zebrafish embryos were transferred from 28°C and manipulated in ice-cold Ca^{2+}-free Ringer solution. For cell cycle inhibition, embryos were treated with nocodazole, 10 μg/ml for 30 min (Sigma). After termination of this treatment, the embryos were washed

with Ca^{2+}-free Ringer solution, 0.05% DMSO (Horowitz et al., 1983), then incubated in egg water for 15 or 30 min. Embryos were dechorionated by pronase, and yolks mechanically disrupted. The embryonic cell mass was then trypsinized, then isolated embryonic cells were stained with propidium iodine, filtered through Cell Strainer Cap (BD), and cell cycle analyzed by fluorescent flow cytometric analyses as previously described (Yarbrough et al., 2002). Cell clusters and debris were manually excluded leaving only isolated single cells for analyses. Cell cycle analyses were performed on a FACSCalibur machine (Becton Dickinson) and analyzed using CellQuest Pro software.

Statistics

Results in graphs represent mean ± SD or as indicated. Statistical significance was determined by unpaired two-tailed Student's t-test (Excel or Prism Software), with $p<0.05$ considered as significant.

Supplementary Material

Refer to Web version on PubMed Central for supplementary material.

Acknowledgments

Grant sponsor: These studies are supported by an endowment to the Barry Baker Laboratories for Head & Neck Oncology, by funds supplied through an Ingram Professorship to WGY, through funds supplied by the Vanderbilt Ingram Cancer Center and the Bill Wilkerson Center for Otolaryngology and Communication Sciences and the Department of Otolaryngology, Vanderbilt University School of Medicine, and through grant # 2R01 DE013173 from the National Institute of Dental and Craniofacial Research (WGY) and in part by the grant # R01 DE018477 from the National Institute of Dental and Craniofacial Research (EWK).

The authors appreciate helpful discussions and comments from the Knapik and Yarbrough Laboratory personnel.

References

Abrams EW, Mullins MC. Early zebrafish development: it's in the maternal genes. Curr Opin Genet Dev. 2009; 19:396–403. [PubMed: 19608405]

Amon A. The spindle checkpoint. Curr Opin Genet Dev. 1999; 9:69–75. [PubMed: 10072359]

An H, Lu X, Liu D, Yarbrough WG. LZAP inhibits p38 MAPK (p38) phosphorylation and activity by facilitating p38 association with the wild-type p53 induced phosphatase 1 (WIP1). PLoS ONE. 2011; 6:e16427. [PubMed: 21283629]

Arendt D, Nubler-Jung K. Rearranging gastrulation in the name of yolk: evolution of gastrulation in yolk-rich amniote eggs. Mech Dev. 1999; 81:3–22. [PubMed: 10330481]

Barrallo-Gimeno A, Holzschuh J, Driever W, Knapik EW. Neural crest survival and differentiation in zebrafish depends on mont blanc/tfap2a gene function. Development. 2004; 131:1463–1477. [PubMed: 14985255]

Bruce AE, Howley C, Dixon Fox M, Ho RK. T-box gene eomesodermin and the homeobox-containing Mix/Bix gene mtx2 regulate epiboly movements in the zebrafish. Dev Dyn. 2005; 233:105–114. [PubMed: 15765511]

Cao Y, Zhao J, Sun Z, Zhao Z, Postlethwait J, Meng A. fgf17b, a novel member of Fgf family, helps patterning zebrafish embryos. Dev Biol. 2004; 271:130–143. [PubMed: 15196956]

Cha YI, Kim SH, Sepich D, Buchanan FG, Solnica-Krezel L, DuBois RN. Cyclooxygenase-1-derived PGE2 promotes cell motility via the G-protein-coupled EP4 receptor during vertebrate gastrulation. Genes Dev. 2006; 20:77–86. [PubMed: 16391234]

Cheng JC, Miller AL, Webb SE. Organization and function of microfilaments during late epiboly in zebrafish embryos. Dev Dyn. 2004; 231:313–323. [PubMed: 15366008]

Ching YP, Qi Z, Wang JH. Cloning of three novel neuronal Cdk5 activator binding proteins. Gene. 2000; 242:285–294. [PubMed: 10721722]

Dosch R, Wagner DS, Mintzer KA, Runke G, Wiemelt AP, Mullins MC. Maternal control of vertebrate development before the midblastula transition: mutants from the zebrafish I. Dev Cell. 2004; 6:771–780. [PubMed: 15177026]

Duffy KT, McAleer MF, Davidson WR, Kari L, Kari C, Liu CG, Farber SA, Cheng KC, Mest JR, Wickstrom E, Dicker AP, Rodeck U. Coordinate control of cell cycle regulatory genes in zebrafish development tested by cyclin D1 knockdown with morpholino phosphorodiamidates and hydroxyprolyl-phosphono peptide nucleic acids. Nucleic Acids Res. 2005; 33:4914–4921. [PubMed: 16284195]

Granero-Molto F, Sarmah S, O'Rear L, Spagnoli A, Abrahamson D, Saus J, Hudson BG, Knapik EW. Goodpasture antigen-binding protein and its spliced variant, ceramide transfer protein, have different functions in the modulation of apoptosis during zebrafish development. J Biol Chem. 2008; 283:20495–20504. [PubMed: 18424781]

Holloway BA, Gomez de la Torre Canny S, Ye Y, Slusarski DC, Freisinger CM, Dosch R, Chou MM, Wagner DS, Mullins MC. A novel role for MAPKAPK2 in morphogenesis during zebrafish development. PLoS Genet. 2009; 5:e1000413. [PubMed: 19282986]

Horowitz MA, Schaffer DB, Diamond GR, Katowitz JA, Quinn GE. Management of traumatic hyphema. JAMA. 1983; 250:3046–3047. [PubMed: 6644984]

Ikegami R, Hunter P, Yager TD. Developmental activation of the capability to undergo checkpoint-induced apoptosis in the early zebrafish embryo. Dev Biol. 1999; 209:409–433. [PubMed: 10328930]

Jeong K, Jeong JY, Lee HO, Choi E, Lee H. Inhibition of Plk1 induces mitotic infidelity and embryonic growth defects in developing zebrafish embryos. Dev Biol. 2010; 345:34–48. [PubMed: 20553902]

Jiang H, Luo S, Li H. Cdk5 activator-binding protein C53 regulates apoptosis induced by genotoxic stress via modulating the G2/M DNA damage checkpoint. J Biol Chem. 2005; 280:20651–20659. [PubMed: 15790566]

Jiang H, Wu J, He C, Yang W, Li H. Tumor suppressor protein C53 antagonizes checkpoint kinases to promote cyclin-dependent kinase 1 activation. Cell Res. 2009; 19:458–468. [PubMed: 19223857]

Joly JS, Joly C, Schulte-Merker S, Boulekbache H, Condamine H. The ventral and posterior expression of the zebrafish homeobox gene eve1 is perturbed in dorsalized and mutant embryos. Development. 1993; 119:1261–1275. [PubMed: 7905819]

Kane DA, Hammerschmidt M, Mullins MC, Maischein HM, Brand M, van Eeden FJ, Furutani-Seiki M, Granato M, Haffter P, Heisenberg CP, Jiang YJ, Kelsh RN, Odenthal J, Warga RM, Nusslein-Volhard C. The zebrafish epiboly mutants. Development. 1996; 123:47–55. [PubMed: 9007228]

Kane DA, Kimmel CB. The zebrafish midblastula transition. Development. 1993; 119:447–456. [PubMed: 8287796]

Kane DA, McFarland KN, Warga RM. Mutations in half baked/E-cadherin block cell behaviors that are necessary for teleost epiboly. Development. 2005; 132:1105–1116. [PubMed: 15689372]

Kimmel CB, Ballard WW, Kimmel SR, Ullmann B, Schilling TF. Stages of embryonic development of the zebrafish. Dev Dyn. 1995; 203:253–310. [PubMed: 8589427]

Kishimoto Y, Koshida S, Furutani-Seiki M, Kondoh H. Zebrafish maternal-effect mutations causing cytokinesis defect without affecting mitosis or equatorial vasa deposition. Mech Dev. 2004; 121:79–89. [PubMed: 14706702]

Lachnit M, Kur E, Driever W. Alterations of the cytoskeleton in all three embryonic lineages contribute to the epiboly defect of Pou5f1/Oct4 deficient MZspg zebrafish embryos. Dev Biol. 2008; 315:1–17. [PubMed: 18215655]

Lin F, Chen S, Sepich DS, Panizzi JR, Clendenon SG, Marrs JA, Hamm HE, Solnica-Krezel L. Galpha12/13 regulate epiboly by inhibiting E-cadherin activity and modulating the actin cytoskeleton. J Cell Biol. 2009; 184:909–921. [PubMed: 19307601]

Ma C, Fan L, Ganassin R, Bols N, Collodi P. Production of zebrafish germ-line chimeras from embryo cell cultures. Proc Natl Acad Sci U S A. 2001; 98:2461–2466. [PubMed: 11226261]

Martinez-Barbera JP, Toresson H, Da Rocha S, Krauss S. Cloning and expression of three members of the zebrafish Bmp family: Bmp2a, Bmp2b and Bmp4. Gene. 1997; 198:53–59. [PubMed: 9370264]

McFarland KN, Warga RM, Kane DA. Genetic locus half baked is necessary for morphogenesis of the ectoderm. Dev Dyn. 2005; 233:390–406. [PubMed: 15768401]

Montero-Balaguer M, Lang MR, Sachdev SW, Knappmeyer C, Stewart RA, De La Guardia A, Hatzopoulos AK, Knapik EW. The mother superior mutation ablates foxd3 activity in neural crest progenitor cells and depletes neural crest derivatives in zebrafish. Dev Dyn. 2006; 235:3199–3212. [PubMed: 17013879]

Montero JA, Kilian B, Chan J, Bayliss PE, Heisenberg CP. Phosphoinositide 3-kinase is required for process outgrowth and cell polarization of gastrulating mesendodermal cells. Curr Biol. 2003; 13:1279–1289. [PubMed: 12906787]

Musacchio A, Hardwick KG. The spindle checkpoint: structural insights into dynamic signalling. Nat Rev Mol Cell Biol. 2002; 3:731–741. [PubMed: 12360190]

Negron JF, Lockshin RA. Activation of apoptosis and caspase-3 in zebrafish early gastrulae. Dev Dyn. 2004; 231:161–170. [PubMed: 15305296]

Pfaff KL, Straub CT, Chiang K, Bear DM, Zhou Y, Zon LI. The zebra fish cassiopeia mutant reveals that SIL is required for mitotic spindle organization. Mol Cell Biol. 2007; 27:5887–5897. [PubMed: 17576815]

Ramel MC, Buckles GR, Baker KD, Lekven AC. WNT8 and BMP2B co-regulate non-axial mesoderm patterning during zebrafish gastrulation. Dev Biol. 2005; 287:237–248. [PubMed: 16216234]

Reim G, Brand M. Maternal control of vertebrate dorsoventral axis formation and epiboly by the POU domain protein Spg/Pou2/Oct4. Development. 2006; 133:2757–2770. [PubMed: 16775002]

Robu ME, Larson JD, Nasevicius A, Beiraghi S, Brenner C, Farber SA, Ekker SC. p53 activation by knockdown technologies. PLoS Genet. 2007; 3:e78. [PubMed: 17530925]

Schulte-Merker S, van Eeden FJ, Halpern ME, Kimmel CB, Nusslein-Volhard C. no tail (ntl) is the zebrafish homologue of the mouse T (Brachyury) gene. Development. 1994; 120:1009–1015. [PubMed: 7600949]

Shimizu T, Yabe T, Muraoka O, Yonemura S, Aramaki S, Hatta K, Bae YK, Nojima H, Hibi M. E-cadherin is required for gastrulation cell movements in zebrafish. Mech Dev. 2005; 122:747–763. [PubMed: 15905076]

Sibon OC, Laurencon A, Hawley R, Theurkauf WE. The Drosophila ATM homologue Mei-41 has an essential checkpoint function at the midblastula transition. Curr Biol. 1999; 9:302–312. [PubMed: 10209095]

Sibon OC, Stevenson VA, Theurkauf WE. DNA-replication checkpoint control at the Drosophila midblastula transition. Nature. 1997; 388:93–97. [PubMed: 9214509]

Sidi S, Goutel C, Peyrieras N, Rosa FM. Maternal induction of ventral fate by zebrafish radar. Proc Natl Acad Sci U S A. 2003; 100:3315–3320. [PubMed: 12601179]

Solnica-Krezel L. Conserved patterns of cell movements during vertebrate gastrulation. Curr Biol. 2005; 15:R213–228. [PubMed: 15797016]

Solnica-Krezel L. Gastrulation in zebrafish -- all just about adhesion? Curr Opin Genet Dev. 2006; 16:433–441. [PubMed: 16797963]

Tang R, Dodd A, Lai D, McNabb WC, Love DR. Validation of zebrafish (Danio rerio) reference genes for quantitative real-time RT-PCR normalization. Acta Biochim Biophys Sin (Shanghai). 2007; 39:384–390. [PubMed: 17492136]

Wagner DS, Dosch R, Mintzer KA, Wiemelt AP, Mullins MC. Maternal control of development at the midblastula transition and beyond: mutants from the zebrafish II. Dev Cell. 2004; 6:781–790. [PubMed: 15177027]

Wang J, An H, Mayo MW, Baldwin AS, Yarbrough WG. LZAP, a putative tumor suppressor, selectively inhibits NF-kappaB. Cancer Cell. 2007; 12:239–251. [PubMed: 17785205]

Wang J, He X, Luo Y, Yarbrough WG. A novel ARF-binding protein (LZAP) alters ARF regulation of HDM2. Biochem J. 2006; 393:489–501. [PubMed: 16173922]

Wilkins SJ, Yoong S, Verkade H, Mizoguchi T, Plowman SJ, Hancock JF, Kikuchi Y, Heath JK, Perkins AC. Mtx2 directs zebrafish morphogenetic movements during epiboly by regulating microfilament formation. Dev Biol. 2008; 314:12–22. [PubMed: 18154948]

Wilm TP, Solnica-Krezel L. Essential roles of a zebrafish prdm1/blimp1 homolog in embryo patterning and organogenesis. Development. 2005; 132:393–404. [PubMed: 15623803]

Yamashita M. Apoptosis in zebrafish development. Comp Biochem Physiol B Biochem Mol Biol. 2003; 136:731–742. [PubMed: 14662298]

Yarbrough WG, Bessho M, Zanation A, Bisi JE, Xiong Y. Human tumor suppressor ARF impedes S-phase progression independent of p53. Cancer Res. 2002; 62:1171–1177. [PubMed: 11861400]

Yin Z, Jones GN, Towns WH 2nd, Zhang X, Abel ED, Binkley PF, Jarjoura D, Kirschner LS. Heart-specific ablation of Prkar1a causes failure of heart development and myxomagenesis. Circulation. 2008; 117:1414–1422. [PubMed: 18316483]

Zamir E, Kam Z, Yarden A. Transcription-dependent induction of G1 phase during the zebra fish midblastula transition. Mol Cell Biol. 1997; 17:529–536. [PubMed: 9001205]

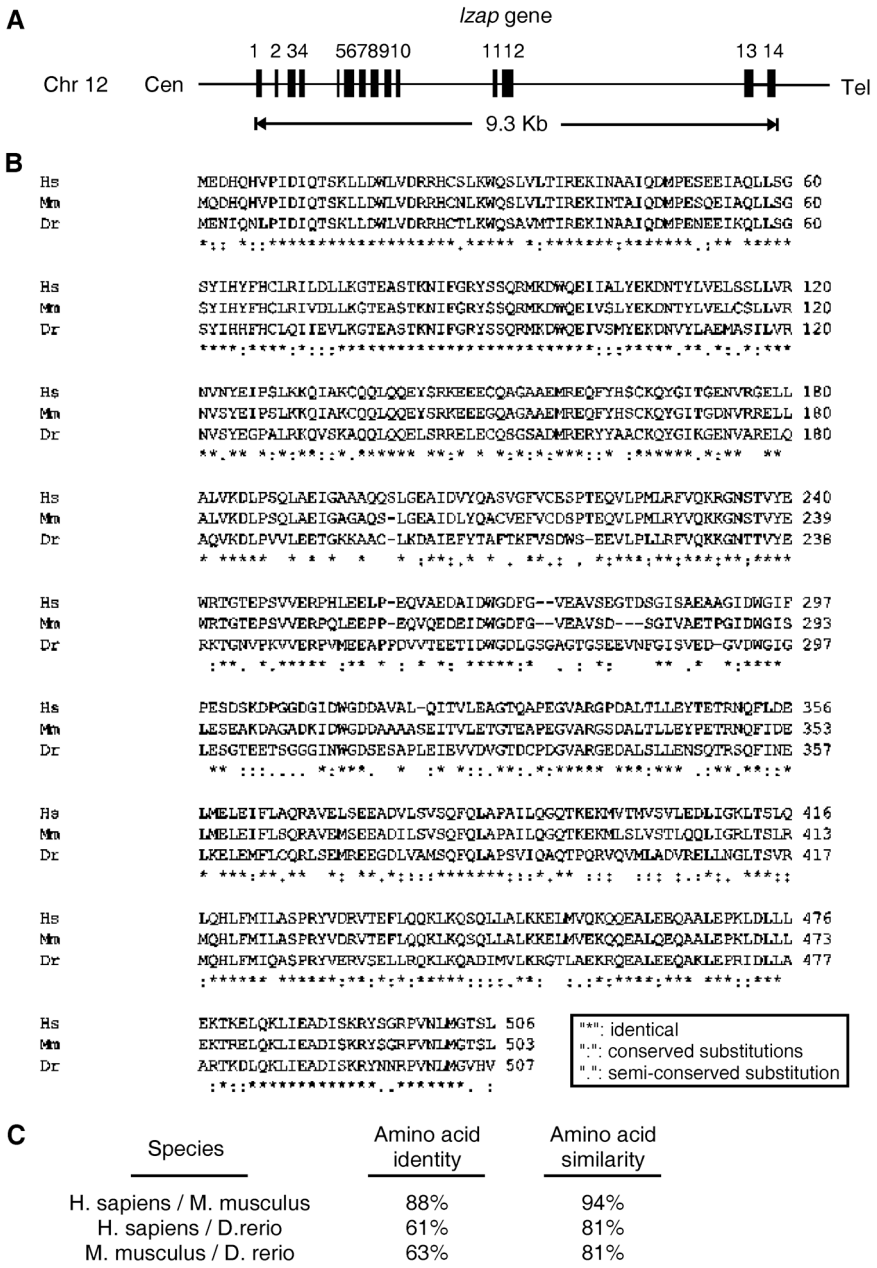

Fig. 1. *lzap* is Highly Conserved During Evolution

A: Gene structure of zebrafish *lzap* located on chromosome 12. Filled boxes represent exons. Cen, centromere; Tel, telomere.

B: Alignment of human, mouse and Zebrafish Lzap protein sequences. Amino acid sequences of Lzap orthologs from the NCBI database were aligned and similarity assigned based on the Clustal W algorithm. Hs, *Homo sapiens* (NP_788276.1); Mm, *Mus musculus* (NP_084524.1); Dr, *Danio rerio* (NP_001002105.1). (✻) identical; (●) conserved; (:) semi-conserved.

C: Pairwise comparison of amino acid conservation between human (H. sapiens), mouse (M. musculus), and zebrafish (D. rerio) Lzap.

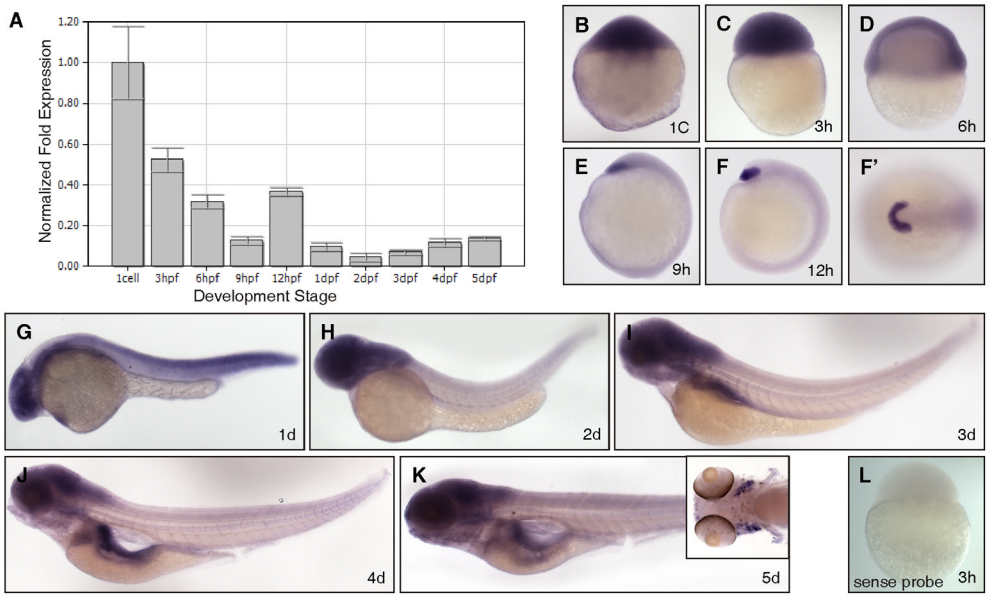

Fig. 2. *lzap* is Expressed during Epiboly and Organogenesis

A: Relative expression of *lzap* mRNA in developing fish embryos. *lzap* expression was determined by qRT-PCR at indicated developmental stages and normalized to *β-actin* expression. hpf, hours post-fertilization; dpf, days post-fertilization.

B–K: Representative photographs of *lzap* expression during development as determined by *in situ* hybridization. Embryos are depicted in lateral view, except for the animal pole view shown in F'. Ubiquitous expression of maternal *lzap* was detected throughout cleavage stages (B, C) and expression was maintained into early epiboly (D). After epiboly from 9–12 hpf, *lzap* expression was concentrated in the precordal plate and areas corresponding to the future hatching gland (E–F'). At 1 dpf to 2 dpf *lzap* expression was more intense in the CNS, eye, and pharyngeal region (G, H). *lzap* staining was visible in the developing pharynx region, pharyngeal arches and in the primordial of the gastrointestinal organs at 3 dpf (I). *lzap* mRNA was detected at 4–5 dpf (J, K) in the pancreas and gastrointestinal tube, jaw and pharynx region, tectum, gills (see inset, K) and the hindbrain regions.

L: Negative control with sense probe at 3 hpf reveals no staining.

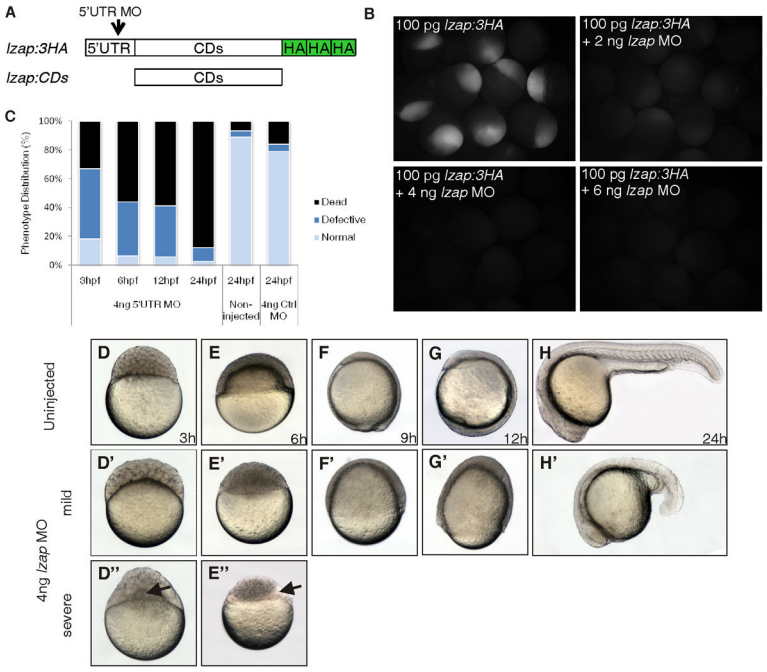

Fig. 3. Morpholino-mediated Depletion of Lzap Results in Cleavage Stage and Epiboly Defects

A: Schematic representation of *lzap* RNAs. *lzap:3HA* contains the 5' UTR sequence targeted by the *lzap* morpholino (MO) and was used to confirm MO effectiveness. *lzap:CDs* contains the entire *lzap* coding sequence but lacks the MO target sequence and was used for rescue.

B: Verification of on-target and dose dependent effects of *lzap* MO on exogenous Lzap expression. Embryos were injected with *lzap:3HA* singly or with increasing amounts of *lzap* MO visualized by immunofluorescence 4-hours post fertilization (hpf). No immunofluorescence was observed in control embryos lacking the primary antibody (data not shown).

C: Schematic showing incidence of developmental defects and non-viable embryos at indicated time points following injection of *lzap* MO, control MO or in embryos without injection.

D–E": *lzap* specific MO or control was injected and viability and morphology determined by microscopic visualization at indicated times. Results were compared to uninjected embryos.

D–H: Lateral view of uninjected embryos from 3–24 hpf.

D'–H', D"–E": Lateral view of *lzap* MO injected embryos. Embryos were time matched to uninjected embryos. Arrows indicate persistence of the syncytial layer. Mild and severe phenotypes following injection of *lzap* MO are shown.

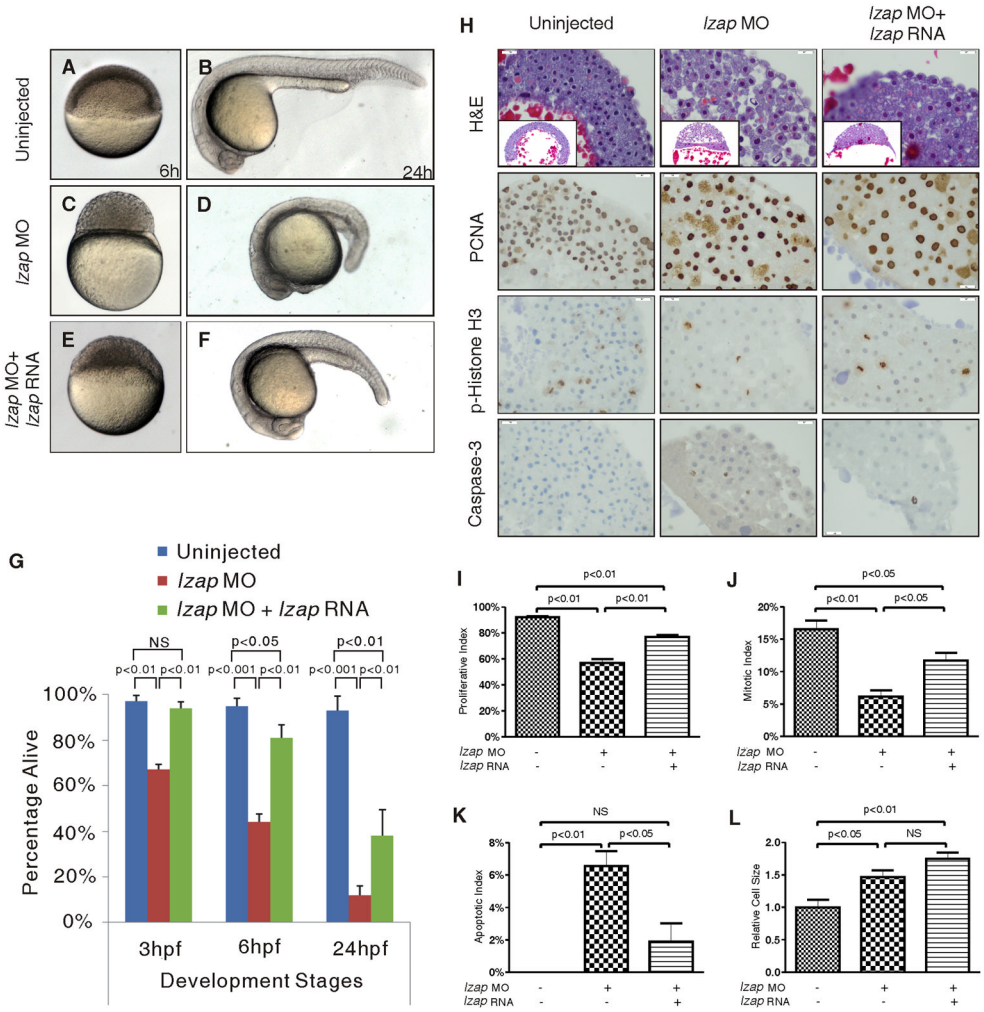

Fig. 4. Cleavage Stage and Epiboly Defects in *lzap* Morphants are Rescued by Co-injection of *lzap* mRNA

A–F: Co-injection of *lzap* mRNA with 5' UTR morpholino (MO) partially rescued developmental defects of *lzap* morphants at 6- and 24-hours post fertilization (hpf).

G: Schematic showing embryo viability at indicated time points following injection of *lzap* MO with or without *lzap* RNA and in embryos without injection. Data represents means and standard errors derived from more than 180 embryos from 3 independent experiments.

H: *lzap* morphants display proliferative, mitotic and apoptotic defects that are partially rescued through co-injection of *lzap* mRNA. Embryos were analyzed at 6 hpf by immunohistochemical staining using antibodies to PCNA, p-Histone H3 and cleaved Caspase-3 as indicated (magnification, ×40).

I–L: Indices for proliferation (I), mitosis (J) and apoptosis (K) were determined by dividing the number of cells staining for PCNA, p-Histone H3, or cleaved Caspase-3, respectively, by the total number of cells. Means and standard error are presented. Data is from sections of 20 independently injected embryos. For relative cell size determination, cell borders were marked on captured hematoxylin stained images and relative area (L) calculated by ImageJ software. Values are normalized to control cells. NS, not significant.

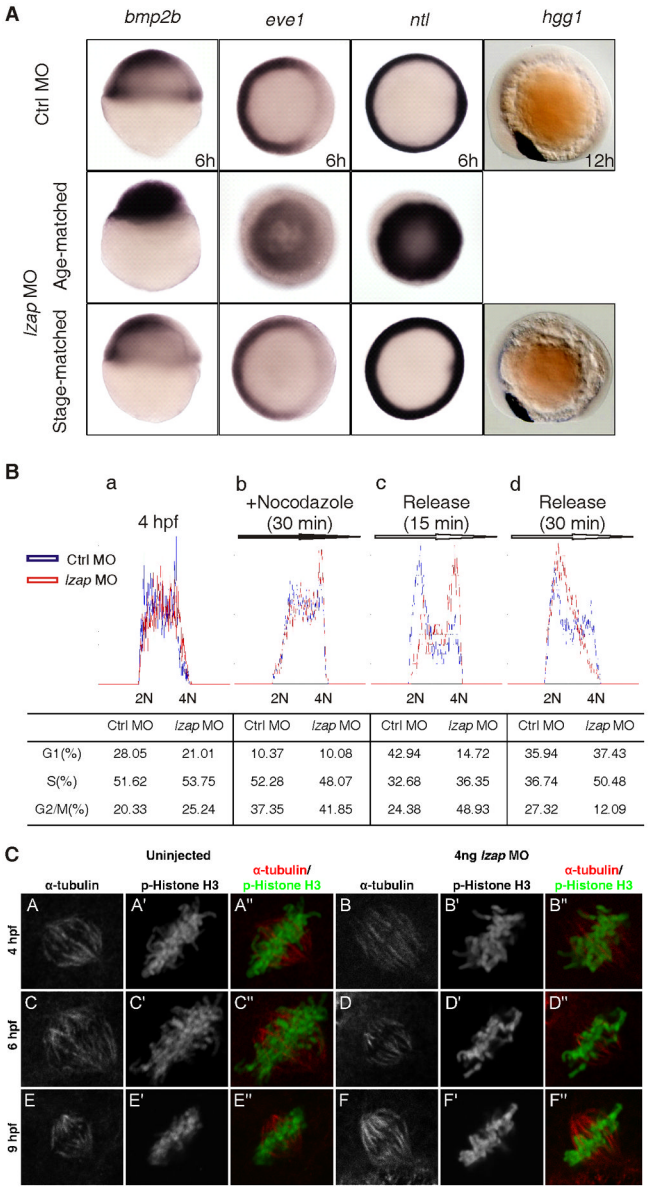

	Ctrl MO	*lzap* MO	Ctrl MO	*lzap* MO	Ctrl MO	*lzap* MO	Ctrl MO	*lzap* MO
G1(%)	28.05	21.01	10.37	10.08	42.94	14.72	35.94	37.43
S(%)	51.62	53.75	52.28	48.07	32.68	36.35	36.74	50.48
G2/M(%)	20.33	25.24	37.35	41.85	24.38	48.93	27.32	12.09

Fig. 5. Depletion of Lzap causes delay in cell cycle progression but does not disrupt zygotic gene expression after MBT

A: The expression of *bmp2b*, *eve1*, *ntl* and *hgg1* in control and both age-matched and stage-matched *lzap* morphant embryos were detected by whole-mount *in situ* hybridization. *bmp2b* expression, lateral view, 6 hpf in control. *eve1* and *ntl* expression, top view, 6 hpf in control. *hgg1* expression, lateral view, 12 hpf in control.

B: Cell cycle analyses of dissociated zebrafish embryonic cells. DNA content was determine on untreated embryonic cells (a), on cells treated with 10 μg/ml nocodazole for 30 min (b), or on cells treated with nocodazole followed by release for 15 (c) or 30 min (d). Cells were assigned to G1, S, or G2/M based on fluorescent signal and manual gating using CellQuest Pro software. Results in the table represent the mean of at least three independent experiments.

C: Embryos with and without injection of 4ng *lzap* MO were co-immunostained with anti-α-tubulin (red) and p-Histone H3 (green) antibodies at 4, 6 and 9 hpf in mitotic cells. Results are representative of observations from more than 100 nuclei for each panel.